Chapter 6
Coil Topology Optimization for Transducers Based on Cylindrical Magnets

6.1 Introduction

The previous chapters have been concerned with the optimization and comparison of eight different coupling architectures in electromagnetic vibration transducers. In summary, geometrical dimensions were found which yield to a maximum output power and output voltage, respectively. The comparison of the maximum performance limits yield the most efficient architectures which should consequently be favoured in the application whenever possible. However a basic characteristic of all the architectures (independent of the architecture class) is that the topology of the coil has always been predefined to be cylindrical. Hence the underlying optimization approach is strictly speaking a sizing optimization. Obviously this makes sense because cylindrical coils, especially made of enamelled copper wire, are state of the art and easy to fabricate. Moreover the optimized dimensions (especially for the "Magnet across coil" architecture class) show that the resulting coils are rather thin. Consequently there is not much space left for an optimization of the coil topology. But for all that an interesting question arises from this:

Is there an axially symmetrical coil topology for an arbitrary cylindrical magnet, which results in a higher output power than a cylindrical coil, and how does it look like?

To answer this question a coil topology optimization procedure was developed which is the topic of this chapter. The chapter is divided into four sections. Section 6.2 introduces the basic idea behind the topology optimization formulation strategy. Section 6.3 presents results of the output power topology optimization based on a predefined cylindrical magnet. To evaluate the performance of the topology optimized coil, architecture A II was chosen as benchmark because it performs best within the architectures based on cylindrical magnets without back iron (refer to Sect. 4.4.1). The chapter concludes with a summary and a discussion of the benefit and the applicability of topology optimized coils. Note that in spite of the previously presented sizing optimization, where the output power and the output voltage are considered separately the topology optimization focuses only on

D. Spreemann and Y. Manoli, *Electromagnetic Vibration Energy Harvesting Devices*, Springer Series in Advanced Microelectronics 35, DOI 10.1007/978-94-007-2944-5_6,

the output power. This is because the limited construction volume condition is no more valid. However, the magnet dimensions must be predefined which results in a variable construction volume. Hence, even coil windings that are very far from a given cylindrical magnet will contribute to the overall output voltage, since the transduction factor is still greater than zero, regardless of the resistance or volume. Consequently a voltage topology optimization would result in huge coils which provide no practical advantage.

6.2 Formulation Strategy

As explained in the introduction, the aim of the topology optimization procedure is to find a coil topology which yields maximum output power based on a given predefined cylindrical magnet. The underlying magnet dimensions used here are adopted from the optimization results of A II ($R_{\mathrm{mag}} = 6$ mm, $h_{\mathrm{mag}} = 7.08$ mm). Moreover, the previous applied boundary conditions (Table 3.2) are still valid. The topology optimization is essentially based on four steps (Table 6.1). First, a global design domain Ω is defined around the magnet such that it is larger than the resulting design. In the calculation example the axis–symmetric design domain range from $x = 0.5$ mm to $x = 12$ mm and from $y = 3.6$ mm to $y = 14$ mm. Note that the distance between the design domain and the magnet is defined by the boundary conditions (gap size of 0.5 mm and maximum inner displacement of 1 mm). Second, the design domain is discretized into n cells. Each cell contains a number of coil windings (dependent on the cell size) which is calculated using (2.25). Third, the cells are evaluated with respect to their output power generation capability and sorted in descending order. The optimized topology is found by starting a virtual winding process which begins at the most efficient cell followed by the second best and so on. After each cell the output power is calculated. As will be shown the output power increases rapidly at the beginning of the virtual winding process. However at a certain point the output power is maximal and decreases with any further cell. At this point the virtual winding process stops and the optimal topology can be interpreted in step 4.

The most complex step in the topology optimization procedure is to evaluate the cells of the global coil design domain. In this regard the most important cell parameters are the transduction factor and the resistance. An ideal cell has a high transduction factor and a small resistance whereas cells with small transduction factors and comparatively high resistances are disadvantageous. The resistance produced by the coil windings in the cells R_{cell} is plotted in Fig. 6.1a. Because the absolute value is dependent on the cell size (discretization refinement) the values are normalized to the maximum cell resistance. The cell resistance is dependent on the total length of wire which is in turn dependent on the x–position of the cell (radius) but not on the y–position. That's why the contour lines are vertical. The generated transduction factor of the cells $k_{\mathrm{t,cell}}$ is plotted in Fig. 6.1b. This plot shows that the windings which are closest to the pole region of the magnet contribute with the highest transduction factors. However, for quantifying the cell evaluation, it

Table 6.1 Illustration of the principal steps applied to find an optimal coil topology

Step 1	Step 2	Step 3	Step 4
Defining global design domain	Discretizing	Finding optimal topology	Interpreting final topology
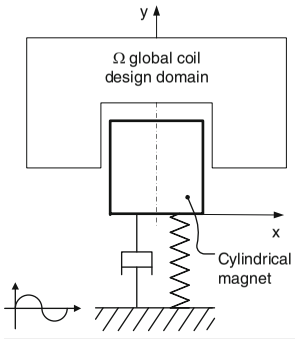	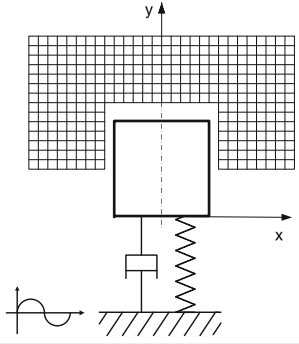	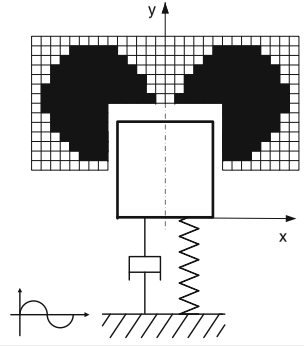	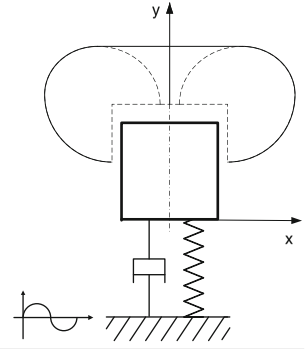

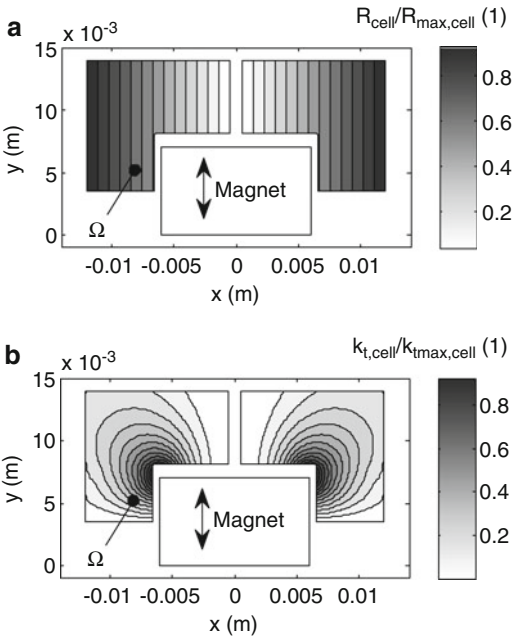

Fig. 6.1 (**a**) Cell resistance and (**b**) transduction factor of the cells in the global design domain

is necessary to know how the output power depends from the resistance and the transduction factor. Based on the analytical analyses the proportionalities of the electromagnetic damping, the optimal load resistance and the inner displacement amplitude are given by:

$$\begin{aligned} d_{e,cell} &\propto \frac{k_{t,cell}^2}{R_{cell} + R_{cell,opt}}, \\ R_{cell,opt} &\propto R_{cell} + k_{t,cell}^2, \\ Z &\propto \frac{1}{\sqrt{1 + \left(\frac{k_{t,cell}^2}{2R_{cell} + k_{t,cell}^2}\right)}}. \end{aligned} \tag{6.1}$$

In addition the proportionalities for the cell *emf* and the voltage divider of the cell resistance and the optimal load resistance of the cell are:

$$\begin{aligned} emf_{cell} &\propto \frac{k_{t,cell}}{\sqrt{1 + \left(\frac{k_{t,cell}^2}{2R_{cell} + k_{t,cell}^2}\right)}}, \\ V_{R_{cell,opt}} &\propto k_{t,cell}^2 \cdot \sqrt{\frac{R_{cell} + k_{t,cell}^2}{2 \cdot k_{t,cell}^2 + 4 \cdot R_{cell}}}. \end{aligned} \tag{6.2}$$

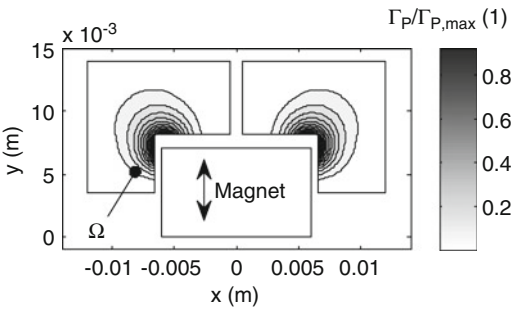

Fig. 6.2 Output power proportionality factor in the global coil design domain

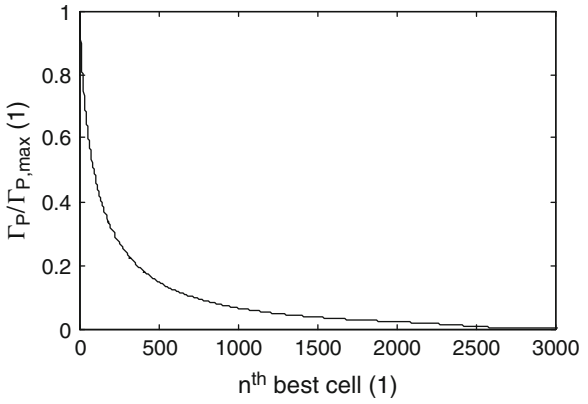

Fig. 6.3 Cells of the global coil design domain sorted in descending order with respect to the output power generation capability

Finally the factor of proportionality for the output power is found to be:

$$P_{cell} \propto \frac{k_{t,cell}^2}{\left(k_{t,cell}^2 + R_{cell}\right)} = \Gamma_P. \tag{6.3}$$

This proportionality factor is used to evaluate the output power capability of the cells. A plot of the output power proportionality factor in the global coil design domain is shown in Fig. 6.2. Due to the increasing resistance in x–direction the isolines of the output power proportionality are slightly bent to the axis of symmetry with respect to the transduction factor. Moreover the result shows that the output power capability of the cells decreases rapidly. This becomes even more apparent if the cells are sorted in descending order (Fig. 6.3).

Now that the most efficient cells in the global coil design domain have been identified the "virtual winding process" starts consequently at the best cell and goes along the cells in descending order. With the total transduction factor and the total resistance:

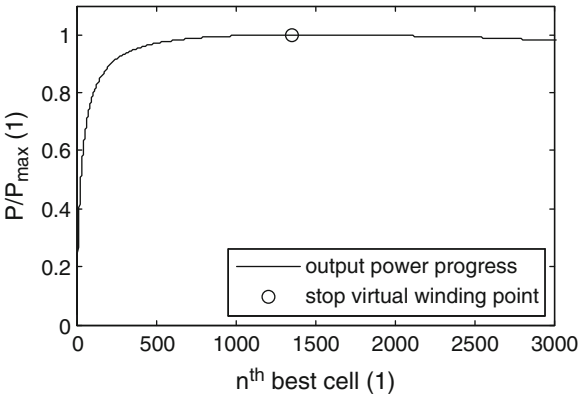

Fig. 6.4 Increase of the output power during the virtual winding process. At cell 1,354 the output power is maximal and the virtual winding process stops

$$k_{t,total} = \sum_{i=1}^{n} k_{t,cell}^{i}$$
$$R_{cell,total} = \sum_{i=1}^{n} R_{cell}^{i}, \tag{6.4}$$

the corresponding progress of the total output power, given by:

$$P_{total} = \sum_{i=1}^{n} P_{cell}^{i} = \sum_{i=1}^{n} \frac{{U_{cell}^{i}}^{2}}{R_{cell,opt}^{i}} = \sum_{i=1}^{n} \frac{\left(k_{t,cell}^{i} \dot{Z}_{cell}^{i}\right)^{2}}{R_{cell}^{i} + \frac{{k_{t,cell}^{i}}^{2}}{d_m}}, \tag{6.5}$$

is shown in Fig. 6.4. In this equation the amplitude of the oscillation velocity is given by:

$$\dot{Z}_{cell}^{i} = \frac{m\omega Y_{acc}}{\sqrt{(k - m\omega^2)^2 + \left(\left(d_m + d_{e,cell}^{i}\right)\omega\right)^2}} \tag{6.6}$$

At cell 1,354 the output power is maximal. Hence the resistance of any further cell is disproportionate to the cell transduction factor. At this point the "virtual winding process" is stopped and the optimal topology can be interpreted in step 4. This is the basic idea behind the formulation strategy. A detailed discussion of the simulation results and the interpretation in step 4 is part of the following section.

6.3 Results of the Topology Optimization

6.3.1 Progress of Important System Parameters

As a basic result the progress of the output power has been used in the last section to explain the formulation strategy and to underline that there is an optimum in the output power during the "virtual winding process". However for more detailed understanding it is necessary to know the progress of other parameters like the resistance, the transduction factor, the *emf* and the electromagnetic damping. The cell resistance is shown in Fig. 6.5. Because the "virtual winding process" starts at the pole region in the global coil design domain and goes along the circular isolines of the output power proportionality it is apparent that the cell resistance starts at a medium value and somehow swings up. However at approximately cell 2,300 the border region of the global coil design domain is reached and the cell resistance cannot exceed the limit which corresponds to the outer radius and cannot fall below the limit which corresponds to the minimum inner radius of the global coil design domain. The cumulative resistance as a sum along the cell resistances together with the optimal load resistance is shown in Fig. 6.6. According to the EDAM the optimal load resistance is obviously greater due to the additional term including the mechanical analog. The cell transduction factor is shown in Fig. 6.7. Because the highest output power proportionalities are in the same region of the global coil design domain as the highest transduction factors the transduction factor starts with the highest values and trends to decrease almost exponentially until the border region is reached and the decrease is almost linear. The cumulative transduction factor is shown in Fig. 6.8. It is apparent that this curve would converge to a horizontal asymptote if the global coil design domain would be further increased. The same characteristic holds for the corresponding *emf* and the output voltage which are shown in Fig. 6.9. This result clearly underlines the statement

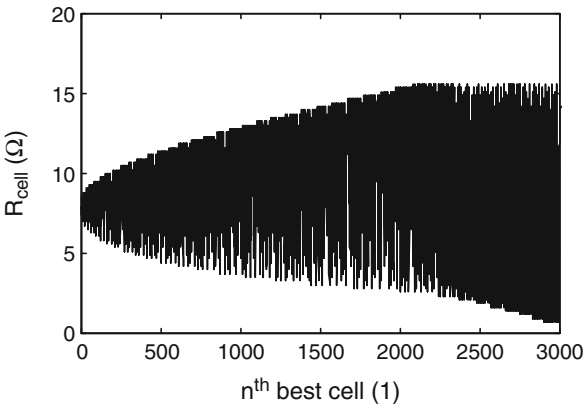

Fig. 6.5 Resistance of the cells

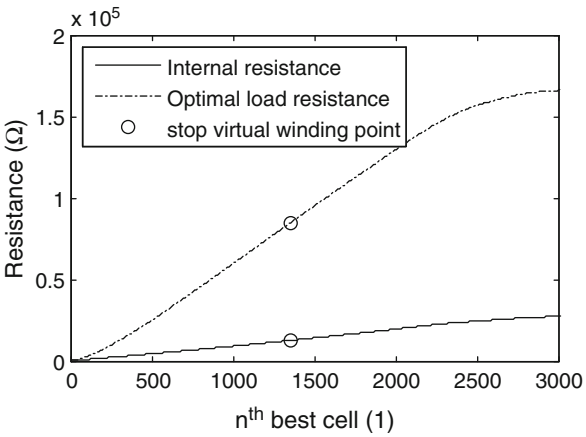

Fig. 6.6 Progress of the cumulative resistance and the optimal load resistance

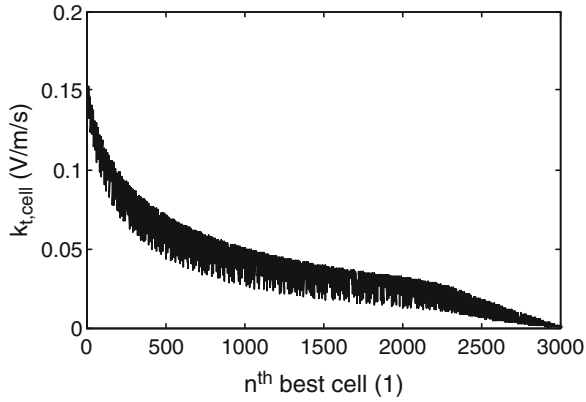

Fig. 6.7 Transduction factor of the cells

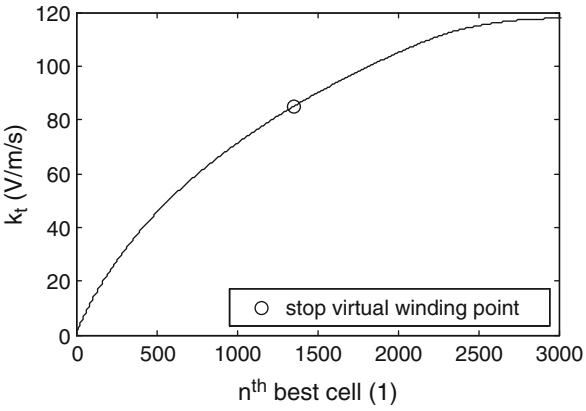

Fig. 6.8 Progress of the cumulative transduction factor during the "virtual winding" process

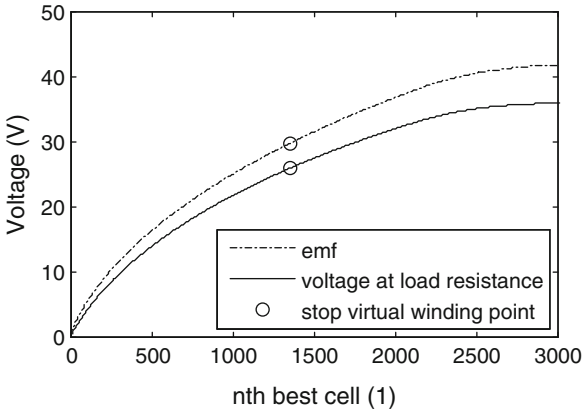

Fig. 6.9 Progress of the cumulative *emf* and the voltage at the optimal load resistance

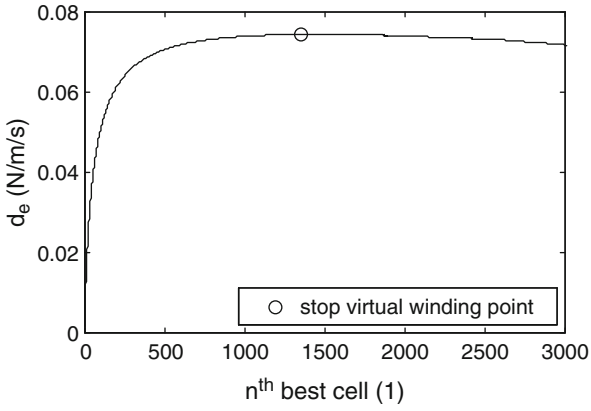

Fig. 6.10 Progress of the electromagnetic damping

mentioned in the introduction that an output voltage optimized topology does not make sense because it would result in huge coils. Another interesting result is the progress of the electromagnetic damping which is shown in Fig. 6.10. Therein the maximum is practically identical with the "stop virtual winding" point and hence also the maximum output power point. Qualitatively this result corresponds to the results from the analytical treatment (Sect. 2.4.2). The reason for this is that the construction volume in the topology optimization is not limited. Hence the seismic mass and the electromagnetic damping are independent in spite of the sizing optimization presented in Chap. 3 where the seismic mass and the electromagnetic damping are not independent (refer also to the calculation example in 2.6 where the maximum electromagnetic damping is identical with the maximum output voltage point). Finally the progress of the inner displacement is shown in Fig. 6.11. Note that the minimum inner displacement amplitude corresponds to the maximum electromagnetic damping and hence also the maximum output power point.

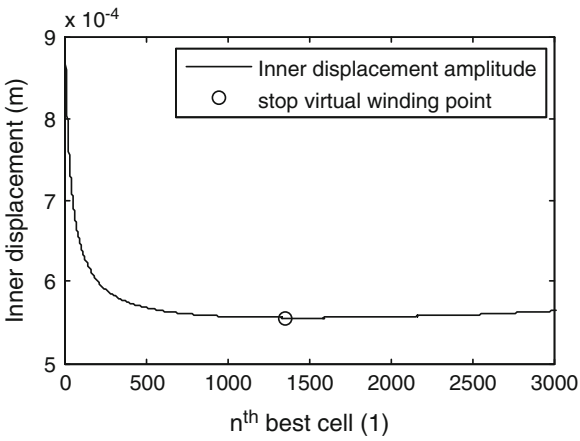

Fig. 6.11 Progress of the inner displacement amplitude

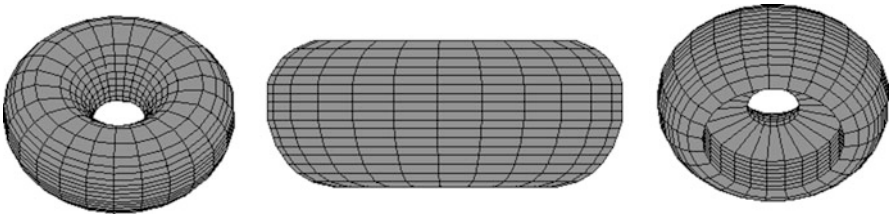

Fig. 6.12 Optimal doughnut–shaped coil topology for a cylindrical magnet. On the *right* picture the recess for the oscillating magnet is visible

6.3.2 Final Interpretation and Performance of the Optimal Topology

In the calculation example the coil topology which yields the maximum possible output power is obtained if the "virtual winding process" goes along the isolines of the output power proportionality factor and stops at the 1,354th best cell. Due to this procedure Fig. 6.2 already denotes the topology of the output power optimized coil. Nevertheless the final interpretation of the topology as a surface of revolution is shown in Fig. 6.12. The topology optimized coil looks somehow like a doughnut–shaped torus with a recess for the magnet. For the given magnet dimensions and boundary conditions this coil yields an output power of 7.89 mW. Note that with respect to the given boundary conditions no other coil is capable of generating a higher output power for the given cylindrical magnet. However the progress of the output power during the virtual winding process shows only a marginal decrease beyond the "stop virtual winding point" (Fig. 6.4). For simplification matters the optimal topology can thus be idealized to a cap like shape without an appreciable loss in the output power (Fig. 6.13). The idealized coil just encompasses the optimal coil. Another advantage of the idealization is that standard fabrication technology for coils made of enamelled copper wires can be used for the manufacturing

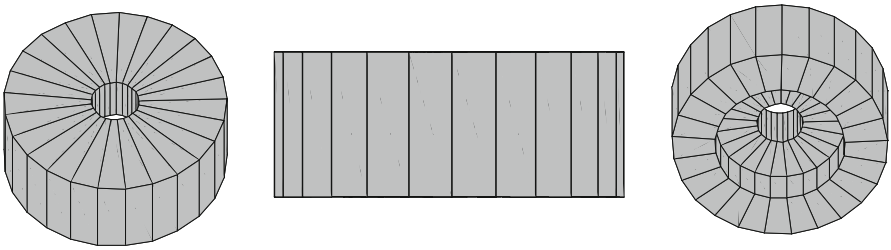

Fig. 6.13 Without an appreciable loss in the output power the optimal coil topology can be idealized to a cap like shape

Fig. 6.14 Topology optimized coils made of enamelled copper wire. The "doughnut" shaped coil (**a**) cannot be fabricated using batch process. The radii are rather imprecise even for customized coils. The idealized cap like coil (**b**) can be batch–fabricated with standard tolerances

in contrast to the "doughnut" shaped coil where the outside radii eliminate the possibility for batch process. Figure 6.14 shows a manufactured customized coil where the outside radii are nevertheless rather imprecise. With the idealized coil the output power reduces negligible to 7.85 mW. However for final evaluation of the performance it is necessary to compare the results to the previous optimization results. For mentioned reasons the benchmark for the topology optimized coil is the architecture A II. After the sizing optimization A II was capable of generating an output power of 4.39 mW (refer to Sect. 4.2.2). Hence with the topology optimization the output power can be increased by approximately 80%. In the first glance this is a considerable increase. However one has to keep in mind that A II is optimized for a construction volume of only 1 cm³. In spite of this the cylindrical construction volume which encompasses the idealized coil and the magnet at the resting position is 4.75 cm³ which is obviously higher. For a final evaluation A II has been optimized again in this larger construction volume. The result shows that for a maximum inner displacement of 1 mm the output power is 22.12 mW. Thus architecture A II is capable of generating almost three times more output power than the topology optimized coil. This is due to the fact that in the topology optimization

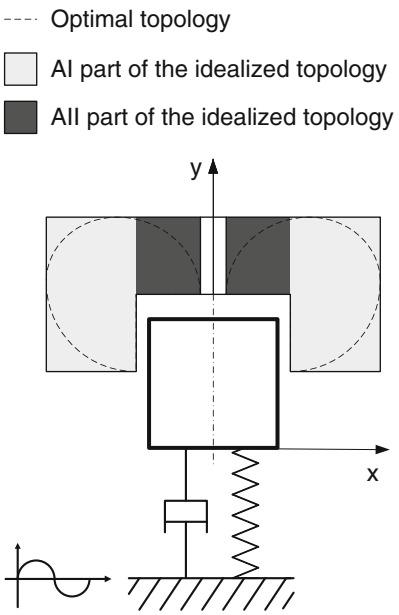

Fig. 6.15 The idealized optimal coil topology is as a combination of the architectures A I and A II

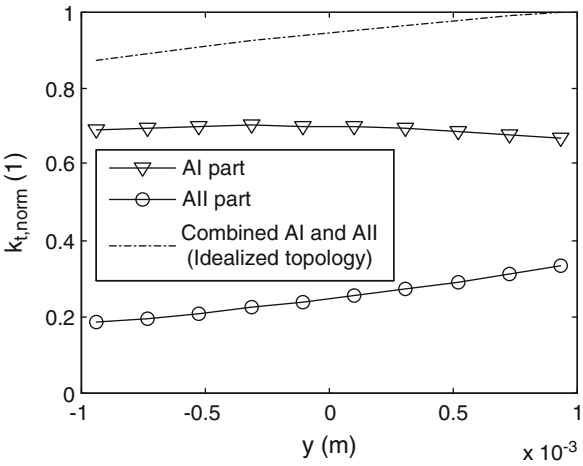

Fig. 6.16 Transduction factor of the idealized coil as a superposition of the A I and the A II part

the magnet dimensions are fixed and the construction volume is variable whereas in the sizing optimization the construction volume is fixed and the dimensions of the magnet are variable which finally results in a better output performance. For a better understanding of this conclusion it is helpful to have a look at the transduction factor. The shape of the idealized optimal coil is in principle a combination of

the architectures A I and A II (Fig. 6.15). Hence the overall transduction factor is a superposition of the separate transduction factors of the A I and the A II part (Fig. 6.16). Even though the A I part contributes with almost 75% of the transduction factor (at the resting position at $y = 0$) it can finally not compensate the loss in weight and magnetic flux gradient if the volume occupied by the windings would be magnetic material. This is consistent with the outcome of the sizing optimization where A II has a considerable better output performance than A I which can be attributed to the fact that in the topology optimization the magnet dimensions are fixed and the construction volume is variable whereas in the sizing optimization of A II the construction volume is fixed and the dimensions of the magnet are variable. For construction volume constrained condition architecture A II finally performs better.

Nevertheless if the specifications in application force fixed magnet dimensions or there is unused space left after the housing of the transducer the results of the topology optimization can be used to maximize the harvested output power. However such specifications are rather untypical which limits the applicability of the topology optimization.